

ARTICLE

Received 21 Aug 2013 | Accepted 18 Nov 2013 | Published 13 Dec 2013

DOI: 10.1038/ncomms3970

OPEN

# Signatures of the electronic nature of pairing in high- $T_c$ superconductors obtained by non-equilibrium boson spectroscopy

Vladimir M. Krasnov<sup>1</sup>, Sven-Olof Katterwe<sup>1,†</sup> & Andreas Rydh<sup>1</sup>

Understanding the pairing mechanism that gives rise to high-temperature superconductivity is one of the longest-standing problems of condensed-matter physics. Almost three decades after its discovery, even the question of whether or not phonons are involved remains a point of contention to some. Here we describe a technique for determining the spectra of bosons generated during the formation of Cooper pairs on recombination of hot electrons as they tunnel between the layers of a cuprate superconductor. The results obtained indicate that the bosons that mediate pairing decay over micrometre-scale distances and picosecond timescales, implying that they propagate at a speed of around  $10^6 \text{ m s}^{-1}$ . This value is more than two orders of magnitude greater than the phonon propagation speed but close to Fermi velocity for electrons, suggesting that the pairing mechanism is mediated by unconventional repulsive electron–electron, rather than attractive electron–phonon, interactions.

<sup>1</sup>Department of Physics, AlbaNova University Center, Stockholm University, SE-10691 Stockholm, Sweden. † Present address: Institut für Luft- und Kältetechnik gemeinnützige Gesellschaft mbH, Bertolt-Brecht-Allee 20, D-01309 Dresden, Germany. Correspondence and requests for materials should be addressed to V.M.K. (email: vladimir.krasnov@fysik.su.se).

Superconductivity is caused by pairing of electrons resulting from virtual exchange of bosons. In low-temperature superconductors Cooper pairing is mediated by phonons, but for high-temperature superconductors the pairing interaction is not yet confidently known<sup>1,2</sup>. There are arguments both in favour of conventional electron–phonon<sup>2–7</sup> and unconventional electron–electron<sup>2,8–16</sup> coupling mechanisms. The electron–phonon coupling in cuprates can be strong because of their ionic structure with high polarizability<sup>17</sup> and poor screening<sup>3,4</sup>. However, it is difficult to reconcile this with a *d*-wave symmetry of the order parameter, which more naturally arises from repulsive electron–electron interactions, for example, via antiferromagnetic magnons<sup>8</sup> or plasmons<sup>10–13</sup>.

In this work, we perform a new type of non-equilibrium boson generation–detection spectroscopy, which allows us to probe the pairing boson. The idea of the experiment is illustrated in Fig. 1a. When non-equilibrium quasiparticles (QPs) are injected into a superconductor through a tunnel junction, they relax to the ground state eventually recombining into Cooper pairs. This inelastic process is accompanied by the emission of bosons that are mediating in pairing. Therefore, identification of recombination bosons provides an unambiguous clue about the pairing glue<sup>18,19</sup>. This has been convincingly shown by similar experiments on low- $T_c$  superconductors<sup>20–23</sup>, in which phonon emission has been detected, reaffirming the electron–phonon pairing mechanism. Here we perform such an experiment on a layered  $\text{Bi}_2\text{Sr}_2\text{CaCu}_2\text{O}_{8+\delta}$  (Bi-2212) cuprate, using natural atomic-scale intrinsic Josephson junctions<sup>24</sup>, both for generation and detection of non-equilibrium bosons. In contrast to the conventional tunnelling spectroscopy, we probe not the single electron current into the sample, but hunt down the emission of non-equilibrium bosons that are responsible for Cooper pairing. We observe that recombination bosons carry a clear spectroscopic information about the superconducting energy gap  $\Delta$ , which reassures the concept of electron–boson coupling with a well-defined pairing glue for cuprates. Analysis of the bosonic decay length yields the boson propagation speed  $\sim 10^6 \text{ ms}^{-1}$  close to the electronic Fermi velocity  $v_F$ . This provides an evidence for the unconventional electron–electron coupling mechanism of high- $T_c$  superconductivity in cuprates.

## Results

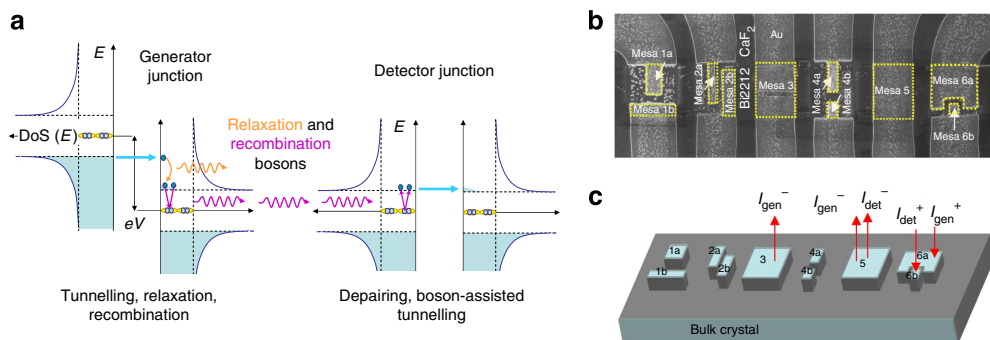
**Sample characteristics.** Figure 1b,c represents the top view and a sketch of the studied sample. It consists of ten small mesa structures of different sizes with attached Au electrodes micro/nanofabricated on top of a slightly underdoped Bi-2212 single

crystal with  $T_c \simeq 81 \text{ K}$ . Mesas contained  $N = 12 \pm 1$  stacked intrinsic Josephson junctions. Each mesa can be biased independently using three or four terminal configuration<sup>18</sup> and can be used either as a generator or a detector. Figure 2a represents a set of current–voltage (*I*–*V*) characteristics of the (generator) mesa 4a at different temperatures. Kinks in the *I*–*V*s at  $T < T_c$  represent sum-gap singularities at  $eV = \pm 2N\Delta$ , see ref. 25.

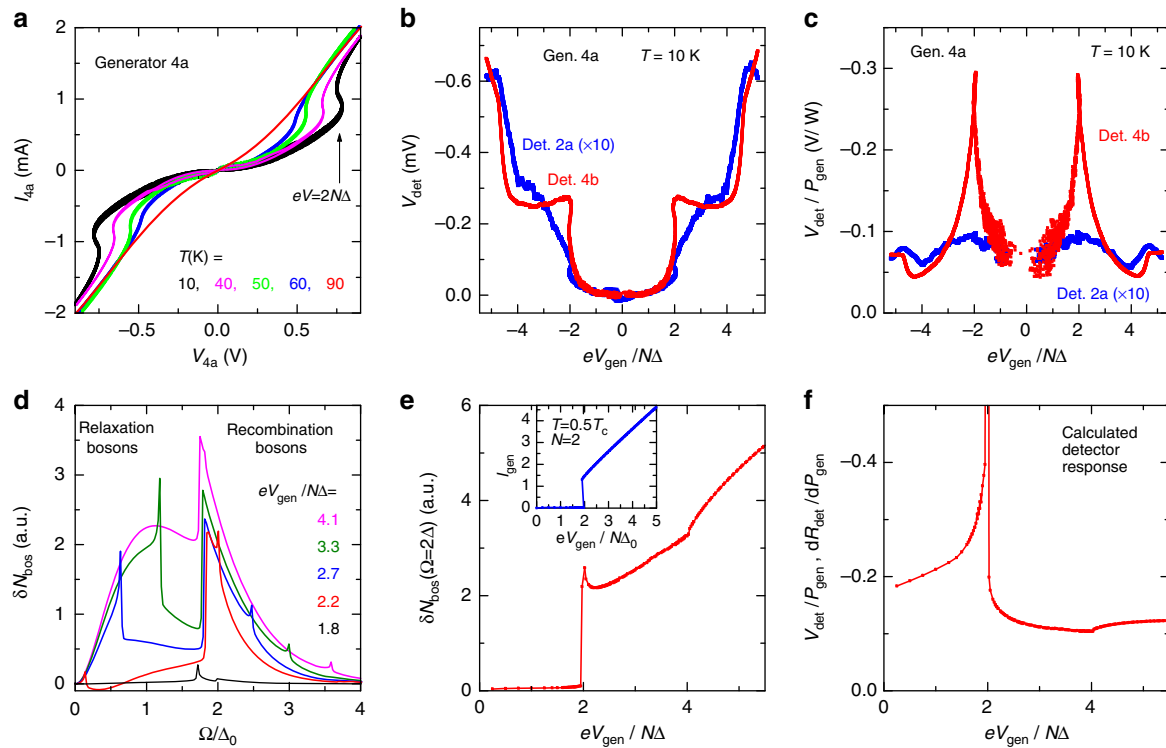
**Generation–detection with unbiased detector.** Figure 2b shows dc-voltages  $V_{\text{det}}$  of unbiased detectors 4b (close to 4a) and 2a ( $\sim 22 \mu\text{m}$  from 4a) as a function of dc-voltage  $V_{\text{gen}}$  in the generator 4a, at  $T = 10 \text{ K}$ . It is seen that a small negative  $V_{\text{det}}$  appears at finite  $V_{\text{gen}}$ . Note that  $V_{\text{det}}$  does not depend on the bias direction of  $V_{\text{gen}}$ . Therefore, there is no direct current injection from the generator into detectors. The detector signal is solely due to reabsorption of uncharged non-equilibrium bosons, which leads to depairing and appearance of excess QPs, as sketched in Fig. 1a. Tunnelling of excess QPs leads to a capacitive charging of unbiased detector junctions, which is measured in the experiment<sup>26</sup>. In this case, the amount of excess QPs and their charge do not depend on the bias direction in the generator. The negative  $V_{\text{det}}$  corresponds to positive charge of carriers, as expected for hole-doped Bi-2212. Note that  $V_{\text{det}}$  is not due to a thermoelectric effect in the base crystal, because the Seebeck coefficient in the superconducting state is zero. Rather, it is similar to a photo-effect in *p*–*n* diodes.

Figure 2c shows  $V_{\text{det}}$  normalized by the generator power  $P_{\text{gen}} = I_{\text{gen}} V_{\text{gen}}$  for the same data. It is seen that the detector response carries a clear spectroscopic information: it peaks at  $eV_{\text{gen}} = 2N\Delta$  and shows a secondary dip/upturn at approximately twice the sum-gap voltage  $eV_{\text{gen}} \simeq 4N\Delta$  (ref. 18; a slight deviation from this equality is caused by slightly different energy gaps in the generator and the detector, see Supplementary Note 1). With increasing the distance from the generator to the detector, the detector response smears out and decays in amplitude. However, spectroscopic features remain recognizable at  $x > 20 \mu\text{m}$  from the generator.

To understand the output of our boson generation–detection experiment, we performed numerical simulations of nonlinear kinetic balance equations for QPs and bosons in stacked Josephson junctions, together with the self-consistency equation for the superconducting gap. Simulations are made for a stack of  $N = 2$  junctions made of ordinary superconductors with an *s*-wave symmetry of the gap at  $T = 0.5 T_c$ . The formalism used is suitable for any type of electron–boson interaction with a well-defined bosonic glue<sup>2</sup>.



**Figure 1 | Outline of the experiment.** (a) Tunnelling diagrams of the generator junction at the sum-gap voltage  $2\Delta < eV < 4\Delta$  and the detector junction at zero bias (*s*-wave case). (b) Scanning electron microscope image of the studied sample. The field of view is  $\sim 60 \times 22 \mu\text{m}^2$ . Ten mesa structures are marked by yellow dotted lines. (c) A three-dimensional sketch of the sample. Arrows indicate a bias configuration with mesa 6a as generator and 6b as detector.



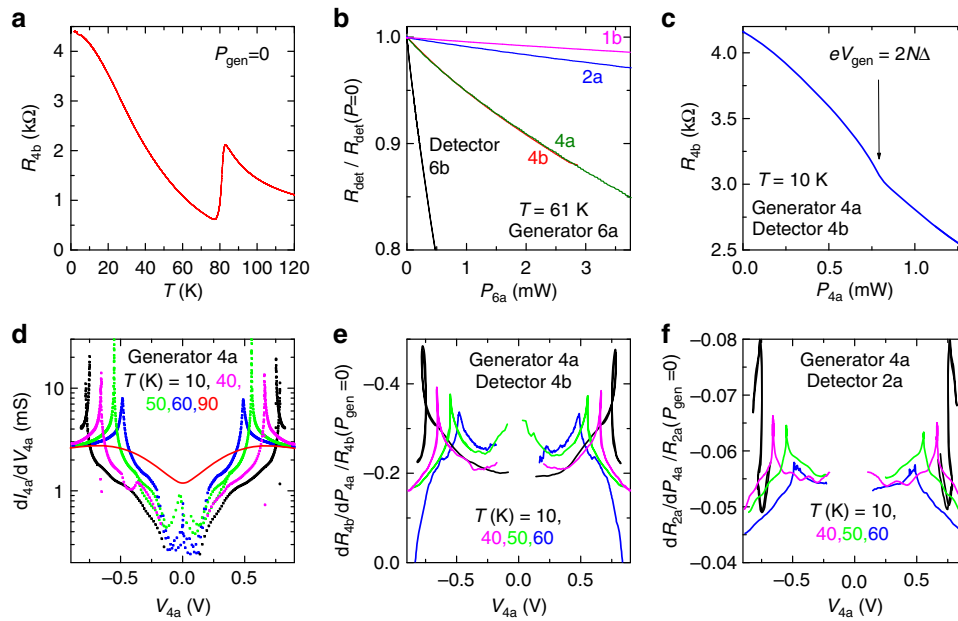
**Figure 2 | Generation-detection with unbiased detector junction and simulated response.** (a) Current-voltage characteristics of mesa 4a with  $N = 12$  junctions. A sum-gap kink is clearly seen at  $T < T_c \approx 81$  K. (b) Voltages of the detector mesas 4b and 2a as a function of voltage in the generator 4a. It is seen that  $V_{\text{det}}$  is independent of the generator bias direction. (c) The detector response normalized by the total power in the generator. Characteristic spectroscopic signatures at  $eV_{\text{gen}}/N \approx 2\Delta$  and  $4\Delta$  are seen. (d-f) Simulation of boson generation-detection experiment (s-wave case). (d) Non-equilibrium boson spectra at different voltages in the generator. Relaxation  $0 < \Omega < eV_{\text{gen}}/N - 2\Delta$  and recombination  $\Omega > 2\Delta$  bands are seen. The bands overlap at  $eV_{\text{gen}}/N = 4\Delta$ . (e) The number of  $\Omega = 2\Delta$  bosons as a function of  $V_{\text{gen}}$ . Inset shows the  $I$ - $V$  of the generator mesa with  $N = 2$  junctions. (f) Normalized detector response  $V_{\text{det}}/P_{\text{gen}} \propto dR_{\text{det}}/dP_{\text{gen}}$  as a function of generator voltage. A primary peak in response at  $eV_{\text{gen}}/N = 2\Delta$  and a secondary dip/upturn at  $eV_{\text{gen}}/N \approx 4\Delta$  indicate onset of pairbreaking by recombination and relaxation bosons, respectively.

Figure 2d shows calculated spectra of generated non-equilibrium bosons for different  $V_{\text{gen}}$  (here  $\Delta_0$  is the equilibrium value of the gap, which is slightly larger than the actual  $\Delta$ , suppressed by the current injection<sup>19</sup>). The corresponding  $I$ - $V$  of the generator is shown in the inset of Fig. 2e. At  $eV_{\text{gen}} > 2N\Delta$ , a large number of non-equilibrium QPs is injected at an energy  $eV_{\text{gen}}/N - 2\Delta$  above the gap. Non-equilibrium QP relaxation usually follows a two-step process<sup>18–22</sup> as sketched in Fig. 1a; first, QPs relax to the edge of the gap, emitting  $\Omega \leq eV_{\text{gen}}/N - 2\Delta$  relaxation bosons, then two QPs form a pair with emission of  $\Omega \geq 2\Delta$  recombination bosons. The corresponding two bosonic bands are seen in Fig. 2d. At  $eV_{\text{gen}}/N = 4\Delta$ , the two bands overlap. Thus, at  $eV_{\text{gen}}/N < 4\Delta$  only recombination bosons have enough energy for pairbreaking, but at  $eV_{\text{gen}}/N > 4\Delta$  an additional depairing will be caused by the high-energy part of relaxation bosons with  $2\Delta \leq \Omega \leq eV_{\text{gen}}/N - 2\Delta$ .

We assume that the detector signal is due to pairbreaking by non-equilibrium  $\Omega \geq 2\Delta$  bosons, which causes excess QP population in the detector and leads to capacitive charging of the detector, similar to a photo-effect in  $p$ - $n$  diodes. In this case, the detector response is proportional to the number of bosons with  $\Omega \geq 2\Delta$  and does not depend on the direction of current in the generator, consistent with our experimental results in Fig. 2b. The main panel of Fig. 2e shows the number of generated non-equilibrium bosons  $\delta N$  with  $\Omega = 2\Delta$  as a function of the generator voltage. Figure 2f shows the calculated detector response, normalized by the generator power. It shows a sharp peak at  $eV_{\text{gen}} = 2N\Delta$  and a secondary dip/upturn at  $eV_{\text{gen}} = 4N\Delta$ .

A sharp increase at  $eV_{\text{gen}} \rightarrow 2N\Delta$  is caused by the sharp onset of recombination boson generation, as shown in Fig. 2e. A sharp drop at  $eV_{\text{gen}} > 2N\Delta$  is caused by a rapid redistribution of the boson spectrum. As seen from Fig. 2d, at  $eV_{\text{gen}} > 2N\Delta$  a significant part of emitted bosons is in the relaxation band with  $\Omega < 2\Delta$ . Those low-energy bosons do not cause depairing and are not detected. This leads to the drop in the detection efficiency. However, at  $eV_{\text{gen}} \geq 4N\Delta$  the upper edge of the relaxation band exceeds  $2\Delta$  and high-energy relaxation bosons start to contribute to depairing<sup>18,20–22</sup>, leading to a secondary upturn in the detector response. The simulated detector responses from Fig. 2e,f can be explicitly compared with experimental data from Fig. 2b,c, correspondingly. A larger smearing of experimental features is likely to be due to the  $d$ -wave symmetry of the order parameter in cuprates (see Supplementary Note 2 and Supplementary Fig. S1). Otherwise, there is a good overall agreement between measured and calculated detector responses.

**Generation-detection with ac-biased detector.** The measurement accuracy can be improved using a lock-in technique. In this case, we send a small ac current through the detector mesa and measure the decrease in ac resistance caused by excess QP population. High sensitivity of this method is due to a strong temperature dependence of the resistance  $R(T)$  (ref. 25) shown in Fig. 3a, which can be used for probing the effective electronic temperature of the detector<sup>27</sup>. Figure 3b shows



**Figure 3 | Generation-detection experiment with ac-biased detector junction.** (a) Temperature dependence of the equilibrium ac resistance of the mesa 4b. (b) Normalized resistances of different detector mesas at  $T = 61$  K as a function of power in the generator mesa 6a. (c) Resistance of the detector mesa 4b at  $T = 10$  K as a function of power in the generator mesa 4a. (d)  $dI/dV(V)$  characteristics of the generator mesa 4a at different  $T$ . Peaks at sum-gap voltages are clearly seen. (e,f) Normalized detector responses of mesas 4b and 2a as a function of voltage in the generator 4a at different  $T$ . Peak responses occur at the sum-gap voltages in the generator.

measured ac resistances of different detector mesas as a function of the power in the generator mesa 6a at  $T = 61$  K. Resistances are normalized to the corresponding equilibrium values at  $P_{\text{gen}} = 0$ . The decrease of  $R_{\text{det}}(P_{\text{gen}})$  indicates the increase of non-equilibrium QP population. The detector response decays rapidly with increasing the distance from the generator. It is largest for the nearest mesa 6b, and smallest for the farthest mesa 1b. The curves for detector mesas 4a and 4b, which have different sizes but are at the same distance from the generator 6a, collapse in one, indicating that the response does not depend on the geometry of the detector but solely on the distance from the generator. As in case of dc measurements in Fig. 2, the ac response does not reduce to a trivial self-heating, but carries a clear spectroscopic information. This is demonstrated in Fig. 3c, which shows the response of the detector 4b to the nearby generator 4a. The arrow indicates a kink in  $R_{\text{det}}(P_{\text{gen}})$ , which is not present in  $R(T)$ . The kink appears when the generator reaches the sum-gap voltage.

Figure 3d represents a set of  $dI/dV$  curves at different  $T$  for the generator 4a. The sum-gap singularities are seen as sharp peaks in conductances<sup>25</sup>. Figure 3e,f represents the corresponding detector responses  $dR_{\text{det}}/dP_{\text{gen}}$ , normalized by the equilibrium value  $R_{\text{det}}(P_{\text{gen}} = 0)$ , as a function of  $V_{\text{gen}}$  (4a), for the detector mesas 4b and 2a. It is seen that detector responses peak at  $eV_{\text{gen}} = \pm 2N\Delta$ , consistent with dc measurements and simulations in Fig. 2c,f. Thus, the detector signal carries a clear spectroscopic information about the superconducting gap. It yields  $\Delta_0 \approx 33$  meV, consistent with previous studies<sup>5,15,25</sup>. This is an important observation, because it proves that pairing bosons have well-defined energies, that is, the ratio of the width of boson level to its energy is small. In the opposite case, the pairing glue would be ill defined<sup>23</sup>. This reassures applicability of the conventional concept of electron-boson coupling to cuprates.

## Discussion

From Figs 2b,c and 3b,e,f, it is seen that the detector response decreases rapidly with increasing the distance from the generator. In Fig. 4a,b we show distance dependence of ac responsivities at zero bias ( $V_{\text{gen}} \rightarrow 0$ ) and at the sum-gap peak ( $eV_{\text{gen}} = 2N\Delta$ ) for different temperatures and generator/detector configurations. In all cases, the detector responsivity decays approximately exponentially with distance at a characteristic decay length  $x_{\tau}$  of several microns.

We want to emphasize that such an exponential decay is not expected in case of simple self-heating<sup>27,28</sup>, that is, in case when the power is simply spread out from the generator without time decay. We demonstrate this in Fig. 4c, which shows calculated temperature distributions at the surface of the crystal for the case of heat diffusion (solid lines) and for partly ballistic phonon transport with a mean free path of  $5 \mu\text{m}$  (dashed lines). Calculations are based on the corresponding analytic expressions (equations 3 and 4 in ref. 28 and equation 3 in ref. 27) for a 3-dimensional  $T$ -distribution from circular mesas with radii  $a = 5$  (thick) and  $1 \mu\text{m}$  (thin lines) on top of a bulk crystal. Despite some differences, at large distances all of them approach a universal  $\delta T_{\text{eff}} \propto 1/r$  dependence, characteristic for heat diffusion from a point source. It is much slower than the observed exponential decay. This indicates that the recombination bosons do not only spread out in the base crystal but also decay with time  $\delta N_{\text{bos}} \propto \exp(-t/\tau)$ , where  $\tau$  is the boson lifetime. This leads to exponential decay of the detector signal with distance, owing to longer time-of-flight to the farthest mesas. It follows that bosons propagate ballistically at an approximately micrometre scale. A certain scattering does take place at larger distances  $> 10 \mu\text{m}$ , as seen from smearing out of the spectroscopic peak in the furthest detector in Fig. 2c.

Relaxation times in cuprates  $\tau \sim 1\text{--}20$  ps are fairly well established via time-resolved optical experiments<sup>16,29–31</sup>. This time represents the inelastic QP relaxation time due to emission

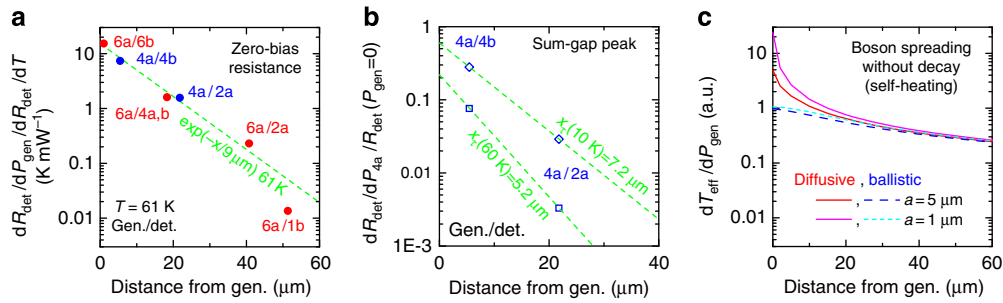


**Figure 4 | Spatial dependence of detector response.** (a) Measured spatial dependence of normalized detector responses at zero-bias  $V_{\text{gen}} \rightarrow 0$  and  $T = 61$  K. (b) Spatial dependencies of peak amplitudes in detector responses at sum-gap voltages in the generator. Note the exponential decay of detector responses with the characteristic decay length  $\lambda_x \sim \mu\text{m}$ . (c) Simulated temperature distribution on heat (phonon) spreading without decay (infinite bosonic lifetime). Note a significantly weaker spatial dependence than in the experiment.

of bosons and the reverse process of boson decay due to absorption by QPs (see also Supplementary Note 3). Using the observed decay length  $\lambda_x$ , we estimate the propagation velocity of recombination bosons  $v_b \sim \lambda_x/\tau \sim 10^6 \text{ m s}^{-1}$ . This velocity is more than two orders of magnitude larger than the phononic sound velocity  $4 \times 10^3 \text{ m s}^{-1}$  (ref. 32) and is close to the electronic Fermi velocity  $v_F$  (ref. 33). Thus, in contrast to low- $T_c$  superconductors<sup>20–22</sup>, the detected pairing boson is not a phonon, but has a pure electronic origin. For comparison, at a similar  $\tau \sim \text{ps}$  phonons would decay at the length scale of a few nanometres, consistent with the observed spatial inhomogeneity of the isotope effect<sup>5</sup>. Therefore, we cannot judge about the role of electron–phonon coupling in cuprates from our data, because the corresponding phonon decay length is well beyond our spatial resolution.

What excitations can propagate at velocities close to  $v_F$ ? Obviously, QPs can do this. However, non-equilibrium QPs would produce  $V_{\text{det}}$  that depends on the charge of injected QPs (electrons or holes), that is, on the direction of the injection current in the generator. Such non-even current response has been observed in previous works with a detector intimately connected with the generator<sup>18,34</sup> (see also a description of the QP signal in Methods). In contrast, in our experiment the detector and the generator are well separated and the detected signal is independent from the bias direction in the generator, as shown in Fig. 2b. This clearly demonstrates that the detector signal is not due to injection of non-equilibrium charge carriers, but is due to inflow of uncharged non-equilibrium bosons. Among bosons, acoustic plasmons can have velocities close to  $v_F$  (refs 10–13). Collective spin waves (antiferromagnetic magnons) can also propagate at a comparable velocity (up to  $\sim 0.5 v_F$ ), as shown by inelastic neutron scattering in cuprates<sup>35</sup>. Because of uncertainty in  $\tau$ , at present we can only exclude phonons but cannot discriminate between plasmons and magnons.

The non-equilibrium boson generation–detection spectroscopy performed here is qualitatively different from conventional tunnelling spectroscopy, because it explicitly detects non-equilibrium recombination bosons emitted on QP relaxation, rather than the electronic current into the sample. This allows hunt down of bosons responsible for pairing. Therefore, our experiment provides evidence for the involvement of unconventional repulsive electron–electron coupling mechanism in high- $T_c$  cuprates, caused by exchange of electronic bosons, such as plasmons or collective spin waves.

## Methods

**Sample fabrication and measurements.** Small mesa structures were fabricated on top of a freshly cleaved Bi-2212 crystal. Shortly after cleaving, a gold protection

layer was deposited and 6-μm-size mesas (such as mesa 3 and 5 in Fig. 1b) were patterned by means of photolithography and ion milling. Finally, some of the mesas were split in two parts and trimmed to smaller sizes by a focused ion beam. More details on sample fabrication can be found in ref. 36. Measurements were performed in a He-flow cryostat at  $T$  down to 1.6 K. The detector responses at several mesas (either dc or ac) were measured simultaneously with the generator  $I$ – $V$  on slow variation of the dc bias in the generator.

**Detection of QP signal.** The response of the detector, which is even with respect to the current direction in the generator, is caused solely by uncharged non-equilibrium bosons. However, an additional signal from QPs, which changes the sign together with the bias in the generator, does exist. This non-even contribution is small at low temperatures, but successively grows as the base temperature approaches  $T_c$ . The QP contribution leads to a minor left–right asymmetry of the detector response in Figs 2 and 3. Close to  $T_c$ , the non-even QP response takes over and dominates the detector signal. The main reason for the smallness of the QP signal lies in the interlayer tunnelling nature of the  $c$  axis transport. In the studied sample, the detector and the generator are separated by an  $\sim 20$ -nm-deep trench. Therefore, non-equilibrium particles on the way from the generator to the detector have to pass through more than ten layers. QPs have a difficulty to do so, because the probability of interlayer tunnelling is small. The probability of a coherent (without scattering) tunnelling through ten layers is a power ten smaller and, therefore, is very small. On the other hand, collective bosonic modes can travel freely within the crystal lattice, for example, phonons, magnons and plasmons can propagate in all directions at distances much larger than the atomic distance. This is essentially the requirement for existence of collective bosonic modes.

**Numerical simulations.** Non-equilibrium distributions of QPs and bosons are described by a system of two coupled kinetic equations:

$$\frac{\partial \delta N(\Omega, E)}{\partial t} = \frac{\partial \delta N}{\partial t_{\text{inj}}} + \frac{\partial \delta N}{\partial t_{\text{rel}}} + \frac{\partial \delta N}{\partial t_{\text{esc}}}, \quad (1)$$

which describes dynamic equilibrium between injection, relaxation and escape of the corresponding particles, respectively. The formalism of electron–boson relaxation in superconductors has been developed in the seminal work by Bardeen, Cooper and Schrieffer. The QP relaxation rate can be written as:

$$\begin{aligned} \frac{\partial \delta N(E)}{\partial t_{\text{rel}}} = & -\frac{4\pi D_{\text{QP}}(0)dE}{\hbar} \\ & \times \int_0^\infty d\Omega \alpha^2(\Omega) D_{\text{B}}(\Omega) \rho(E) \rho(E+\Omega) A(E, E+\Omega) \{f(E)[1-f(E+\Omega)]g(\Omega) \\ & - f(E+\Omega)[1-f(E)][1+g(\Omega)]\} \\ & + \int_0^{E-\Delta} d\Omega \alpha^2(\Omega) D_{\text{B}}(\Omega) \rho(E) \rho(E-\Omega) A(E, E-\Omega) \{f(E)[1-f(E-\Omega)] \\ & \times [1+g(\Omega)] - f(E-\Omega)[1-f(E)]g(\Omega)\} \\ & + \int_{E+\Delta}^\infty d\Omega \alpha^2(\Omega) D_{\text{B}}(\Omega) \rho(E) \rho(\Omega-E) B(E, \Omega-E) \{f(E)f(\Omega-E) \\ & \times [1+g(\Omega)] - [1-f(E)][1-f(\Omega-E)]g(\Omega)\}. \end{aligned} \quad (2)$$

Here,  $D_{\text{QP}}(0)$  is the electronic density of states per spin at Fermi level in the volume of the electrode,  $D_{\text{B}}(\Omega)$  is the boson density of states per ion,  $\rho(E)$  is normalized by  $D_{\text{QP}}(0)$  QP density of states,  $\alpha^2(\Omega)$  is the electron–boson spectral function,  $A(E, E_2) = 1 - \frac{\Delta^2}{E_1 E_2}$  and  $B(E, E_2) = 1 + \frac{\Delta^2}{E_1 E_2}$  are the coherence factors,

and  $f(E)$  and  $g(\Omega)$  are the non-equilibrium occupation numbers for QPs and bosons, respectively. The first integral in equation (2) describes net scattering of QPs upwards with absorption of a boson, the second integral describes net relaxation with emission of a boson and the third integral describes pairbreaking and recombination.

Non-equilibrium bosons are produced on relaxation of non-equilibrium QPs, that is, there is an exact balance between boson excitation and QP relaxation. Therefore, the boson relaxation rate is opposite to the QP relaxation rate and can be written as

$$\begin{aligned} \frac{\partial \delta N(\Omega)}{\partial t_{\text{rel}}} &= -\frac{8\pi D_{\text{QP}}(0)z^2(\Omega)D_{\text{B}}(\Omega)d\Omega}{\hbar} \\ &\times \int_{\Delta}^{\infty} dE \rho(E)\rho(E+\Omega)A(E, E+\Omega)\{f(E)[1-f(E+\Omega)]g(\Omega) \\ &- f(E+\Omega)[1-f(E)][1+g(\Omega)]\} + \frac{1}{2} \int_{\Delta}^{\infty} dE \rho(E)\rho(\Omega-E)B(E, \Omega-E) \\ &\times \{[1-f(E)][1-f(\Omega-E)]g(\Omega) - f(E)f(\Omega-E)[1+g(\Omega)]\} \end{aligned} \quad (3)$$

In the first integral, the two terms describe destruction and creation of bosons due to absorption by QPs and relaxation of QPs, respectively. In the second integral, the two terms describe destruction of bosons due to absorption by Cooper pairs (pairbreaking) and creation of recombination bosons on pairing of QPs, respectively. The factor 1/2 in front of the second integral reflects the fact that two QPs produce one boson on recombination into the Cooper pair.

To accurately describe non-equilibrium phenomena at large injection currents, it is necessary to take into account the influence of non-equilibrium QP distribution on the superconducting gap. The energy gap  $\Delta$  is connected to the QP distribution  $f(E)$  (no matter equilibrium or not) via the self-consistency equation:

$$\frac{1}{\lambda} = \int_{\Delta}^{\Omega_{\text{D}}} \frac{1-2f(E)}{\sqrt{E^2-\Delta^2}} dE. \quad (4)$$

Here,  $\lambda$  is the electron–boson coupling constant and  $\Omega_{\text{D}}$  is the effective bosonic cutoff (Debye) energy. In general, this equation describes the suppression of  $\Delta$  on increase of  $f(E)$ ; however, due to the denominator under the integral in equation (4) the gap is most sensitive to QPs at the edge of the gap  $E = \Delta$ .

Non-equilibrium QPs are injected in electrodes via tunnel junctions. The QP injection rate is proportional to the tunnelling current:

$$\frac{\partial \delta N(E)}{\partial t_{\text{inj}}} = \frac{\Delta}{e^2 R_{\text{n}}} \rho(E)\rho(E-eV)[f(E-eV) - f(E)] \frac{dE}{\Delta}, \quad (5)$$

where  $V$  is the bias voltage (per junction) and  $R_{\text{n}}$  is the tunnel (normal) resistance of the junction. Note that this equation is also nonlinear, because  $\Delta$  depends on  $f$  via the self-consistency equation.

Finally, it is necessary to specify the QP and boson escape rates. Here, stacking of junctions in the generator has an important role and enhances non-equilibrium effects both in QP and boson subsystems. For QPs, the escape from inner electrodes is effectively blocked by the presence of adjacent tunnel junctions. Bosons, to the contrary, may freely travel in the crystal lattice and are thus collective for the whole stack. This leads to a cascade amplification of the non-equilibrium boson population proportional to the number of junctions in the stack<sup>18</sup>. The simulations presented in Fig. 2 were made for the minimal model of  $N = 2$  stacked Josephson junctions with one inner electrode. All the characteristics are shown for the inner electrode and thus catch the main stacking effects. In the simulations, we assumed that the QP escape rate from the middle electrode is zero, whereas the boson escape rate is just proportional to the impingement rate at the interface with a finite (50%) transmission probability.

We numerically solved the full nonlinear system of two coupled integral equations (1–3) together with the self-consistency equation (4), following the iterative finite difference procedure described in the Supplementary Material to ref. 19. It should be clarified that Fig. 1a represents only the most probable two step decay process, in which the QP first relaxes to the edge of the gap, emitting a relaxation boson, and then two QPs recombine into a Cooper pair, emitting a recombination boson. Probabilities of such processes are enhanced by the singularities in the QP density of states. However, from equations (2) and (3), it is seen that there are many other processes as well, such as reabsorption of an equilibrium boson by non-equilibrium QP, multistep QP relaxation with emission of low-energy bosons, recombination between any two QPs and creation of secondary non-equilibrium QPs due to pairbreaking. All those possibilities are taken into account on solving the nonlinear integral (equations (1–3)).

## References

- Leggett, A. J. What do we know about high Tc? *Nat. Phys.* **2**, 134–136 (2006).
- Carbotte, J. P., Timusk, T. & Hwang, J. Bosons in high-temperature superconductors: an experimental survey. *Rep. Prog. Phys.* **74**, 066501 (2011).
- Abrikosov, A. A. Theory of high-Tc superconducting cuprates based on experimental evidence. *Int. J. Mod. Phys.* **13**, 3405–3418 (1999).
- Alexandrov, A. S., Samson, J. H. & Sica, G. High-temperature superconductivity from realistic Coulomb and Fröhlich interactions. *Europhys. Lett.* **100**, 17011 (2012).
- Lee, J. *et al.* Interplay of electron–lattice interactions and superconductivity in  $\text{Bi}_2\text{Sr}_2\text{CaCu}_2\text{O}_{8+\delta}$ . *Nature* **442**, 546–550 (2006).
- Park, S. R. *et al.* Angle-resolved photoemission spectroscopy of electron-doped cuprate superconductors: isotropic electron-phonon coupling. *Phys. Rev. Lett.* **101**, 117006 (2008).
- Johnston, S. *et al.* Systematic study of electron-phonon coupling to oxygen modes across the cuprates. *Phys. Rev. B* **82**, 064513 (2010).
- Monthoux, P., Balatsky, A. V. & Pines, D. Toward a theory of high-temperature superconductivity in the antiferromagnetically correlated cuprate oxides. *Phys. Rev. Lett.* **67**, 3448–3451 (1991).
- Norman, M. R. & Pepin, C. The electronic nature of high temperature cuprate superconductors. *Rep. Prog. Phys.* **66**, 1547–1610 (2003).
- Rietschel, H. & Sham, L. J. Role of electron Coulomb interaction in superconductivity. *Phys. Rev. B* **28**, 5100–5108 (1983).
- Bill, A., Morawitz, H. & Kresin, V. Z. Electronic collective modes and superconductivity in layered conductors. *Phys. Rev. B* **68**, 144519 (2003).
- Atwal, G. S. & Ashcroft, N. W. Polarization waves and superconducting instabilities in electron systems. *Phys. Rev. B* **70**, 104513 (2004).
- Pashitskii, E. A. & Pentegov, V. I. On the plasmon mechanism of high- $T_{\text{c}}$  superconductivity in layered crystals and two dimensional systems. *Low Temp. Phys.* **34**, 113–122 (2008).
- Niestemski, F. C. *et al.* A distinct bosonic mode in an electron-doped high-transition-temperature superconductor. *Nature* **450**, 1058–1061 (2007).
- Pasupathy, A. N. *et al.* Electronic origin of the inhomogeneous pairing interaction in the high-Tc superconductor  $\text{Bi}_2\text{Sr}_2\text{CaCu}_2\text{O}_{8+\delta}$ . *Science* **320**, 196–201 (2008).
- Dal Conte, S. *et al.* Disentangling the electronic and phononic glue in a high- $T_{\text{c}}$  superconductor. *Science* **335**, 1600–1603 (2012).
- Katterwe, S. O., Motzkau, H., Rydh, A. & Krasnov, V. M. Coherent generation of phonon-polaritons in  $\text{Bi}_2\text{Sr}_2\text{CaCu}_2\text{O}_{8+x}$  intrinsic Josephson junctions. *Phys. Rev. B* **83**, 100510(R) (2011).
- Krasnov, V. M. Quantum cascade phenomenon in  $\text{Bi}_2\text{Sr}_2\text{CaCu}_2\text{O}_{8+\delta}$  single crystals. *Phys. Rev. Lett.* **97**, 257003 (2006).
- Krasnov, V. M. Nonlinear nonequilibrium quasiparticle relaxation in Josephson junctions. *Phys. Rev. Lett.* **103**, 227002 (2009).
- Eisenmenger, W. & Dayem, A. H. Quantum generation and detection of incoherent phonons in superconductors. *Phys. Rev. Lett.* **18**, 125–127 (1967).
- Dayem, A. H. & Wiegand, J. J. Emitted phonon spectrum and its influence on the detected signal in superconducting Sn diodes. *Phys. Rev. B* **5**, 4390–4403 (1972).
- Dynes, R. C. & Narayanamurti, V. Phonon fluorescence in superconductors and the propagation characteristics of high-frequency phonons in Ge: Sb and  $\text{Al}_2\text{O}_3: \text{V}^{3+}$ . *Phys. Rev. B* **6**, 143–171 (1972).
- Dayem, A. H., Miller, B. I. & Wiegand, J. J. Phonon generation and detection in superconducting lead diodes. *Phys. Rev. B* **3**, 2949–2961 (1971).
- Kleiner, R. & Müller, P. Intrinsic Josephson effects in high- $T_{\text{c}}$  superconductors. *Phys. Rev. B* **49**, 1327–1341 (1994).
- Krasnov, V. M. Temperature dependence of the bulk energy gap in underdoped  $\text{Bi}_2\text{Sr}_2\text{CaCu}_2\text{O}_{8+\delta}$ : evidence for the mean-field superconducting transition. *Phys. Rev. B* **79**, 214510 (2009).
- Smith, A. D., Tinkham, M. & Skocpol, W. J. New thermoelectric effect in tunnel junctions. *Phys. Rev. B* **22**, 4346–4354 (1980).
- Krasnov, V. M., Sandberg, M. & Zogaj, I. *In situ* measurement of self-heating in intrinsic tunneling spectroscopy. *Phys. Rev. Lett.* **94**, 077003 (2005).
- Krasnov, V. M., Yurgens, A., Winkler, D. & Delsing, P. Self-heating in small mesa structures. *J. Appl. Phys.* **89**, 5578–5580 (2001).
- Demsar, J., Podobnik, B., Kabanov, V. V., Wolf, T. h. & Mihailovic, D. Superconducting gap  $\Delta_{\text{c}}$ , the pseudogap  $\Delta_{\text{p}}$ , and pair fluctuations above  $T_{\text{c}}$  in overdoped  $\text{Y}_{1-x}\text{Ca}_x\text{Ba}_2\text{Cu}_3\text{O}_{7-\delta}$  from femtosecond time-domain spectroscopy. *Phys. Rev. Lett.* **82**, 4918–4921 (1999).
- Gedik, N. *et al.* Abrupt Transition in quasiparticle dynamics at optimal doping in a cuprate superconductor system. *Phys. Rev. Lett.* **95**, 117005 (2005).
- Saichu, R. P. *et al.* Two-component dynamics of the order parameter of high temperature  $\text{Bi}_2\text{Sr}_2\text{CaCu}_2\text{O}_{8+\delta}$  superconductors revealed by time-resolved raman scattering. *Phys. Rev. Lett.* **102**, 177004 (2009).
- Wu, J. *et al.* Elastic constants and observation of significant elastic softening in superconducting  $\text{Bi}_2\text{Sr}_2\text{CaCu}_2\text{O}_8$  single crystals. *Phys. Rev. B* **47**, 2806–2811 (1993).
- Chiao, M. *et al.* Low-energy quasiparticles in cuprate superconductors: a quantitative analysis. *Phys. Rev. B* **62**, 3554–3558 (2000).
- Rother, S. *et al.* Charge-imbalance effects in intrinsic Josephson systems. *Phys. Rev. B* **67**, 024510 (2003).
- Fujita, M. *et al.* Progress in neutron scattering studies of spin excitations in high-Tc cuprates. *J. Phys. Soc. Jpn* **81**, 011007 (2012).

36. Jacobs, T. h. *et al.* Electron-tunneling measurements of low- $T_c$  single-layer  $\text{Bi}_{2+x}\text{Sr}_{2-y}\text{CuO}_{6+\delta}$ : Evidence for a scaling disparity between superconducting and pseudogap states. *Phys. Rev. B* **86**, 214506 (2012).

### Acknowledgements

Financial support from the Swedish Research Council and technical support from the Core facility in Nanotechnology at Stockholm University are gratefully acknowledged. We are thankful to A.V. Balatsky for valuable remarks.

### Author contributions

S.-O.K. manufactured the samples. S.O.K., V.M.K. and A.R. carried out the measurements. V.M.K. designed the experiment, analysed the data and carried out the simulations. V.M.K. wrote the first draft of the manuscript. All the authors contributed to writing the manuscript.

### Additional information

**Supplementary Information** accompanies this paper at <http://www.nature.com/naturecommunications>.

**Competing financial interests:** The authors declare no competing financial interests.

**Reprints and permission** information is available online at <http://npg.nature.com/reprintsandpermissions/>

**How to cite this article:** Krasnov, V. M. *et al.* Signatures of the electronic nature of pairing in high- $T_c$  superconductors obtained by non-equilibrium boson spectroscopy. *Nat. Comm.* 4:2970 doi: 10.1038/ncomms3970 (2013).



This work is licensed under a Creative Commons Attribution-NonCommercial-ShareAlike 3.0 Unported License. To view a copy of this license, visit <http://creativecommons.org/licenses/by-nc-sa/3.0/>